

# The influence of surfaces on the transient terahertz conductivity and electron mobility of GaAs nanowires

Hannah J Joyce<sup>1</sup>, Sarwat A Baig<sup>1</sup>, Patrick Parkinson<sup>2</sup>,  
Christopher L Davies<sup>3</sup>, Jessica L Boland<sup>3</sup>, H Hoe Tan<sup>4</sup>,  
Chennupati Jagadish<sup>4</sup>, Laura M Herz<sup>3</sup> and Michael B Johnston<sup>3</sup>

<sup>1</sup> Department of Engineering, University of Cambridge, Electrical Engineering Building, 9 JJ Thomson Avenue, Cambridge, CB3 0FA, United Kingdom

<sup>2</sup> School of Physics and Astronomy, University of Manchester, Manchester, M13 9PL, United Kingdom

<sup>3</sup> Department of Physics, University of Oxford, Clarendon Laboratory, Parks Road, Oxford OX1 3PU, United Kingdom

<sup>4</sup> Department of Electronic Materials Engineering, Research School of Physics and Engineering, The Australian National University, Canberra ACT 2601, Australia

E-mail: [hannah.joyce@eng.cam.ac.uk](mailto:hannah.joyce@eng.cam.ac.uk)

Received 4 November 2016

Accepted for publication 31 March 2017

Published 9 May 2017



CrossMark

## Abstract

Bare unpassivated GaAs nanowires feature relatively high electron mobilities (400–2100  $\text{cm}^2 \text{V}^{-1} \text{s}^{-1}$ ) and ultrashort charge carrier lifetimes (1–5 ps) at room temperature. These two properties are highly desirable for high speed optoelectronic devices, including photoreceivers, modulators and switches operating at microwave and terahertz frequencies. When engineering these GaAs nanowire-based devices, it is important to have a quantitative understanding of how the charge carrier mobility and lifetime can be tuned. Here we use optical-pump–terahertz-probe spectroscopy to quantify how mobility and lifetime depend on the nanowire surfaces and on carrier density in unpassivated GaAs nanowires. We also present two alternative frameworks for the analysis of nanowire photoconductivity: one based on plasmon resonance and the other based on Maxwell–Garnett effective medium theory with the nanowires modelled as prolate ellipsoids. We find the electron mobility decreases significantly with decreasing nanowire diameter, as charge carriers experience increased scattering at nanowire surfaces. Reducing the diameter from 50 nm to 30 nm degrades the electron mobility by up to 47%. Photoconductivity dynamics were dominated by trapping at saturable states existing at the nanowire surface, and the trapping rate was highest for the nanowires of narrowest diameter. The maximum surface recombination velocity, which occurs in the limit of all traps being empty, was calculated as  $1.3 \times 10^6 \text{ cm s}^{-1}$ . We note that when selecting the optimum nanowire diameter for an ultrafast device, there is a trade-off between achieving a short lifetime and a high carrier mobility. To achieve high speed GaAs nanowire devices featuring the highest charge carrier mobilities and shortest lifetimes, we recommend operating the devices at low charge carrier densities.

Keywords: GaAs, nanowire, diameter, mobility, lifetime, terahertz, surface

(Some figures may appear in colour only in the online journal)



Original content from this work may be used under the terms of the [Creative Commons Attribution 3.0 licence](https://creativecommons.org/licenses/by/3.0/). Any further distribution of this work must maintain attribution to the author(s) and the title of the work, journal citation and DOI.

## 1. Introduction

GaAs, one of the most extensively used semiconductors, underpins a variety of applications ranging from high frequency electronics and communications systems to high efficiency photovoltaics. GaAs nanowires combine the advantages of the GaAs material system with the advantages of the nanowire geometry, such as efficient lateral strain relaxation, optical waveguiding, enhanced light trapping and emission, and reduced cost and materials consumption relative to conventional planar geometries [1]. These advantages have seen GaAs nanowires and associated heterostructures used in efficient solar cells [1, 2], single photon sources [3], lasers [4] and ultrafast terahertz photodetectors [5].

The electrical properties of unpassivated GaAs nanowires are strongly affected by midgap states at the surface of the nanowires [6]. These surface states are responsible for the high surface recombination velocities ( $>10^5$  cm s<sup>-1</sup>) and the ultrashort charge carrier lifetimes ( $<5$  ps) common to GaAs nanowires [7]. These effects are often regarded as undesirable and are commonly mitigated by overcoating the nanowires with a passivating AlGaAs shell [8]. Nevertheless, unpassivated GaAs nanowires can retain reasonable charge carrier mobilities [9, 10], which together with their ultrashort charge carrier lifetimes make these nanowires suitable for ultrafast devices, such as fast photodetectors and high frequency modulators and switches.

To engineer these types of devices, we require a quantitative understanding of the electrical properties of the unpassivated nanowires and the influence of nanowire surfaces on these properties. Attaining this information using conventional contact-based and optical techniques has proven challenging and consequently unpassivated GaAs nanowires are not as well-characterised as their passivated counterparts [8, 11–13]. Photoluminescence (PL) studies, for example, have been limited to cryogenic temperatures due to the poor quantum efficiencies of unpassivated GaAs nanowires [8, 14, 15]. GaAs nanowires are notoriously difficult to form Ohmic electrical contacts with, because the required high temperature annealing steps cause decomposition of the nanowires and because of significant charge carrier depletion due to surface states [16]. This has hampered electrical characterisation of the nanowires and significant effort is currently being invested in improving electrical contacts to GaAs nanowires [17–19].

In this contribution we use a less conventional technique, optical-pump–terahertz-probe (OPTP) spectroscopy, to study the electrical properties of the unpassivated GaAs nanowires. OPTP spectroscopy does not require either electrical contacts to nanowires or the emission of light from nanowires, overcoming the difficulties associated with both contact-based measurements and PL measurements. Our previous work demonstrated that OPTP spectroscopy can achieve the sub-picosecond temporal resolution necessary for measuring ultrashort lifetimes in GaAs nanowires [7, 10]. By studying nanowires of different diameters, we disentangle the effects of the nanowire surface on both charge carrier mobility and charge carrier lifetime. We also present two alternative models for the analysis of nanowire photoconductivity: the plasmon

resonance model and Maxwell–Garnett effective medium theory with the nanowires approximated as prolate ellipsoids.

## 2. Experimental methods

### 2.1. Nanowire growth

GaAs nanowires were grown on GaAs (1 1 1)B substrates via metal–organic vapour phase epitaxy using gold nanoparticles to drive nanowire growth according to the vapour–liquid–solid mechanism. Arsine (AsH<sub>3</sub>) and trimethylgallium precursors were used at a V/III ratio of 46. Growth was performed using a two-temperature process with growth temperature of 375 °C and a total growth time of 15 min [20]. This growth process was chosen to achieve minimally tapered nanowires with uniform diameters and twin-free zinc-blende crystal structure [20]. Samples were grown using Au nanoparticles of three different sizes to achieve three separate samples with average diameters of 30 nm, 50 nm and 80 nm. Scanning electron microscope images of the three samples are shown in figure 1. The standard deviation in nanowire diameter was less than 10% for each sample.

The nanowires investigated feature smooth {1 1 2} side-facets with surface roughness less than 1 nm, as determined by transmission electron microscopy [21]. We have previously shown that annealing transforms the nanowire facets from {1 1 2} to {1 1 0} [21], but that this {1 1 2}-to-{1 1 0} facet change is not associated with any significant change in charge carrier lifetime or mobility [12]. Therefore, the measurements presented here are broadly applicable to GaAs nanowires with {1 1 2} or {1 1 0} facets.

### 2.2. Optical-pump–terahertz-probe spectroscopy

After growth the nanowires were transferred from the growth substrates to z-cut quartz substrates. These quartz substrates are suitable for OPTP measurements because they are transmissive over a window of 0–3.8 THz and they exhibit no photoconductivity response to obscure the response of the nanowires.

OPTP measurements were performed using a system described in our previous work [22]. Briefly, the nanowire samples were photoexcited with an optical laser pulse, then probed with a terahertz pulse of bandwidth 0.1–4 THz. The system measures the electric field,  $E$  of the terahertz pulse transmitted through the sample, and the change in transmission,  $\Delta E$ , induced by photoexcitation. The relative change in transmission,  $\Delta E/E$ , is directly related to the photoinduced conductivity, or photoconductivity,  $\Delta\sigma$ , of the nanowires. In this study the GaAs nanowires were photoexcited with laser pulses centred at 800 nm (1.55 eV) of 35 fs duration and fluences between 4 and 100  $\mu\text{J}/\text{cm}^2/\text{pulse}$ .

The system provides two principal types of measurements: photoconductivity spectra and photoconductivity decays. Photoconductivity spectra measure the frequency-dependent photoconductivity at a particular time after photoexcitation, and are exemplified in figure 2. Photoconductivity decays, on the other hand, record the photoconductivity as a function of

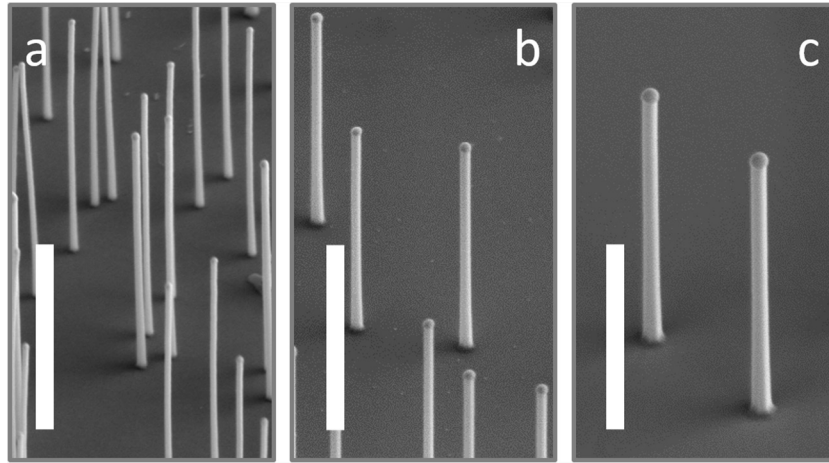


**Figure 1.** SEM images of GaAs nanowires grown with diameters of (a) 30 nm, (b) 50 nm and (c) 80 nm. Images were taken at a tilt of 40°. Scale bars are 1 μm.

time after photoexcitation. Further details can be found in our recent publication [23].

### 2.3. Calculating the conductivity of the nanowires

We consider that the nanowires are confined in a layer of thickness  $d$ , in which the nanowires occupy a fill factor of  $f$  and are surrounded by vacuum. The transmitted electric fields with and without optical photoexcitation are respectively,

$$E_{\text{on}} = fE_w^* + (1 - f)E_v, \quad (1)$$

$$E_{\text{off}} = fE_w + (1 - f)E_v. \quad (2)$$

Here,  $E_w$  is the electric field transmitted through the nanowires and  $E_v$  is the field transmitted through the remaining vacuum, and  $*$  denotes the field transmitted when the nanowires are photoexcited. As the underlying quartz substrate is very thick and the layer containing the nanowires is very thin compared with the terahertz wavelength, the following equations relating  $E_w^*$ ,  $E_v$  and  $E_w$  can be derived:

$$\frac{E_w}{E_v} = \frac{1 + \tilde{n}_s}{1 + \tilde{n}_s - \frac{i\omega d}{c}(\epsilon_w + \tilde{n}_s)}, \quad (3)$$

$$\frac{E_w^*}{E_w} = \frac{1 + \tilde{n}_s - \frac{i\omega d}{c}(\epsilon_w + \tilde{n}_s)}{1 + \tilde{n}_s - \frac{i\omega d}{c}(\epsilon_w^* + \tilde{n}_s)}, \quad (4)$$

where  $\omega$  is the frequency,  $c$  is the speed of light,  $\tilde{n}_s$  is the complex refractive index of the quartz substrate, and  $\epsilon_w$  and  $\epsilon_w^*$  are the complex dielectric functions of the nanowires with and without photoexcitation, respectively. The derivations for equations (3) and (4) can be found in the appendix. By combining these equations and noting that  $\epsilon_w^* - \epsilon_w = i\Delta\sigma/\omega\epsilon_0$ , and  $\Delta E = E_{\text{on}} - E_{\text{off}}$ , we obtain:

$$\Delta\sigma = -\frac{\epsilon_0 c}{d}(A - 1) \left( 1 + \tilde{n}_s - \left[ \frac{i\omega d}{c}(\epsilon_w + \tilde{n}_s) \right] \right), \quad (5)$$

where

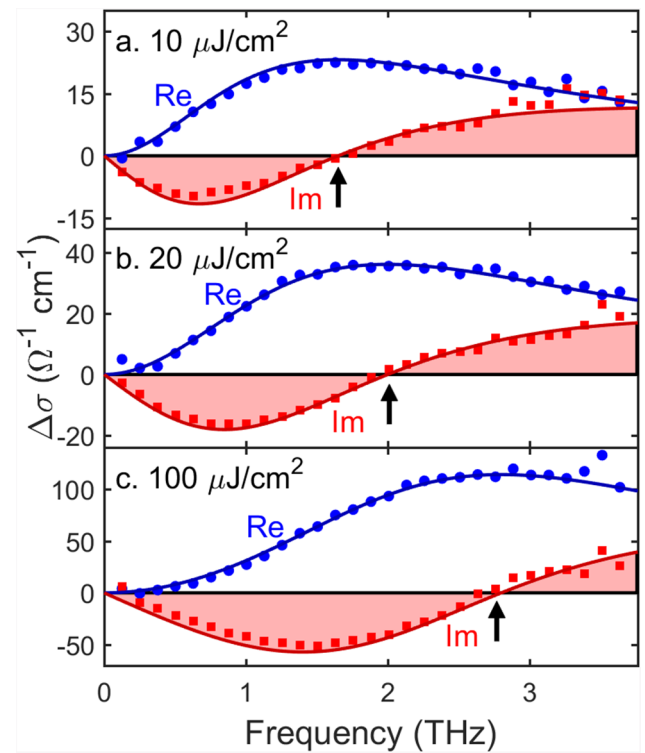


**Figure 2.** Photoconductivity spectra of GaAs nanowires with average diameters of 80 nm. Spectra were taken at 2 ps after photoexcitation with photoexcitation fluences of (a) 10, (b) 20 and (c) 100 μJ cm<sup>-2</sup>. The symbols are the measured data and the lines are the fitted plasmon responses. The real (blue circles and lines) and imaginary (red squares and lines) components of the conductivity are plotted. Vertical black arrows show the position of the resonant frequency,  $\omega_0$ .

$$A = \left( \frac{\Delta E}{E_{\text{off}}} \left( \left( \frac{1}{f} - 1 \right) \left[ \frac{i\omega d}{c} \frac{(\epsilon_w + \tilde{n}_s)}{1 + \tilde{n}_s} \right] + \frac{1}{f} \right) + 1 \right)^{-1}. \quad (6)$$

The terms in the square brackets in equations (5) and (6) are typically small for semiconductor nanowires lying horizontally on the substrate. Furthermore, the quantity  $\frac{\Delta E}{E_{\text{off}}}$  is generally small. Under these conditions the equation simplifies to:

$$\Delta\sigma = -\frac{\epsilon_0 c}{d} \frac{1}{f} \frac{\Delta E}{E_{\text{off}}} (1 + \tilde{n}_s), \quad (7)$$

as given by Strait *et al* [24].

Fill factors,  $f$ , were measured from scanning electron micrographs of the nanowires on the quartz substrates. Photoconductivity spectra were then calculated from the measured  $\frac{\Delta E}{E_{\text{off}}}$  using equation (5).

### 3. Results and discussion

#### 3.1. Nanowire conductivity spectra

Conductivity spectra provide information on charge carrier mobility and the charge carrier scattering processes occurring in the nanowires. All analyses were performed assuming that in the first 5 ps, the measured photoconductivity arises predominantly from photoexcited electrons, as the electron effective mass is significantly lower than the hole effective mass. This assumption is discussed further in section 3.3. The conductivity spectra did not exhibit any measurable signatures of free carriers introduced by unintentional dopants. The negligible contribution of doping to conductivity is expected given the high purity of intrinsic GaAs nanowires grown at low temperature and high V/III ratio [20, 25], and given that the presence of midgap surface states cause significant depletion throughout the GaAs nanowire volume [16].

Photoconductivity spectra were measured after photoexcitation with fluences between 4 and 100  $\mu\text{J cm}^{-2}$ , and between 1 ps and 5 ps after photoexcitation. Figure 2 illustrates typical photoconductivity spectra, which feature strong Lorentzian lineshapes in the terahertz frequency range. This response arises from longitudinal plasmon oscillations and follows

$$\Delta\sigma(\omega) = \frac{nq^2}{m^*} \frac{i\omega}{\omega^2 - \omega_0^2 + i\omega\gamma}, \quad (8)$$

where  $n$  is the photoexcited electron density,  $q$  is the electronic charge,  $m^*$  is the electron effective mass in GaAs and  $\omega_0$  is the resonant frequency. The spectra were fitted with equation (8), as illustrated in figure 2. The same spectral shape is obtained considering an alternative approach combining Maxwell–Garnett effective medium theory and the Drude model [23]. Using this alternative approach, it can be shown that the resonant frequency is given by

$$\omega_0 = \sqrt{\frac{(1-f)}{B} \frac{nq^2}{m^* \epsilon_0}}, \quad (9)$$

where

$$B = -f(\epsilon_w - \epsilon_h) + \left( \epsilon_w + \frac{1-L}{L} \epsilon_h \right). \quad (10)$$

Here,  $\epsilon_h$  is the dielectric constant of the host medium (vacuum) surrounding the nanowires and  $L$  is the depolarisation factor along the elongated axis of the nanowire. Equation (9) reflects the dependence of  $\omega_0$  on the square root of the carrier density  $n$ , which is a characteristic of plasmon resonance. The shift of  $\omega_0$  with increasing carrier density is evident in the spectra of figure 2.

No closed-form solution exists for the depolarisation factor of nanowires, but Venermo and Sihvola demonstrated that cylindrical geometries can be accurately modelled as ellipsoids, for which a closed-form solution exists [26]. Accordingly, we model the nanowires as prolate ellipsoids with a diameter-to-length aspect ratio of  $R$ . The depolarisation factor along the nanowire axis is

$$L = \frac{1-e^2}{e^2} \left( \frac{1}{2e} \ln \frac{1+e}{1-e} - 1 \right) \quad (11)$$

where

$$e = \sqrt{1-R^2}. \quad (12)$$

According to equations (9)–(12) above, the resonant frequency  $\omega_0$  increases (i) with increasing carrier density  $n$ , (ii) with increasing nanowire diameter, and (iii) with decreasing nanowire length. The same trends have been observed in Si nanowires by Chou and Filler [27]. The GaAs nanowires, once transferred to quartz, feature lengths between 1 and 2  $\mu\text{m}$ , and diameters between 30 nm and 80 nm. With these dimensions and the investigated photoexcited carrier densities as input parameters, we used equations (9)–(12) to calculate theoretical resonant frequencies  $\omega_0$  between 0.2 THz and 4.5 THz. This range of frequencies is in good agreement with the resonances observed experimentally.

#### 3.2. Electron mobility and diameter

Each photoconductivity spectrum was fitted with the plasmon model of equation (8) with  $N$ ,  $\omega_0$  and  $\gamma$  as free parameters. The momentum scattering rate was converted to electron mobility via

$$\mu = \frac{q}{m^* \gamma}. \quad (13)$$

The electron mobilities and scattering rates measured for the three different samples are plotted in figure 3. For each sample the mobility decreases with increasing carrier density, due to the increased rate of carrier–carrier scattering at higher photoexcited carrier densities. The mobility shows a strong systematic dependence on the diameter of the nanowires, with nanowires of narrower diameter exhibiting smaller mobilities. This dependence indicates that scattering at the nanowire surface, due to charged surface states and surface roughness, strongly affects the electron mobility in GaAs nanowires. The degradation is stronger in nanowires of smaller diameters in which a greater fraction of free charge carriers interact with the surface.

We employ the Caughey–Thomas equation to describe the empirical relationship between mobility and charge carrier density:

$$\mu(n) = \mu_{\text{min}} + \frac{\mu_{\text{max}} - \mu_{\text{min}}}{1 + \left( \frac{n}{n_{\text{ref}}} \right)^\alpha}. \quad (14)$$

In this empirical equation,  $n_{\text{ref}}$  is the carrier density at which  $\mu$  is midway between  $\mu_{\text{max}}$  and  $\mu_{\text{min}}$ , and the exponent  $\alpha$  describes the shape of the curve. To fit the data obtained



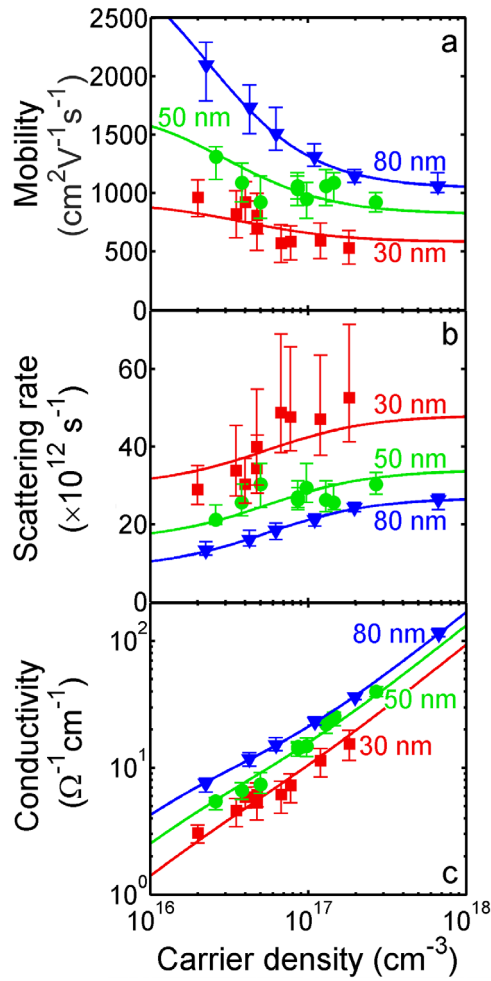


**Figure 3.** (a) Electron mobilities, (b) electronic scattering rates and (c) peak conductivities measured at various photoexcited electron densities for GaAs nanowires with diameters of 30 nm (red squares), 50 nm (green circles) and 80 nm (blue triangles). The error bars indicate the range of values that give adequate fits to the spectra. The fitted lines are based on the empirical Caughey–Thomas equation with additional scattering contributions due to the interaction of electrons with the nanowire surface.

from the narrower-diameter (30 nm and 50 nm) nanowires we included additional scattering components to account for the increased influence of scattering at the nanowire surfaces. We assume this additional component follows Mattheissen’s rule:

$$\gamma_{\text{total}} = \gamma_{\text{bulk}} + \gamma_{\text{surface}}, \quad (15)$$

where  $\gamma_{\text{bulk}}$  is the scattering rate in bulk GaAs and  $\gamma_{\text{surface}}$  is the additional momentum scattering rate due to interactions with the nanowire surface. All the data were globally fitted with equation (14) subject to the constraint of equation (15). The fits are plotted in figure 3 and the fit parameters are summarised in table 1.

The data were fitted well under the assumption that surface-related scattering rates are independent of charge carrier density. Compared to the 80 nm diameter nanowires, the 50 nm diameter nanowires suffer additional surface-related scattering at a rate of  $7 \times 10^{12} \text{ s}^{-1}$ , and the 30 nm diameter nanowires feature an additional scattering rate of  $20 \times 10^{12} \text{ s}^{-1}$ . In the diameter range of 30–80 nm, each 10 nm reduction in diameter

**Table 1.** Caughey–Thomas fit parameters describing the electron mobilities of GaAs nanowires of diameter 30 nm, 50 nm and 80 nm. The fits were performed subject to the constraint of Mattheissen’s rule in equation (15).

Diameter (nm)	$\mu_{\text{min}}$ ( $\text{cm}^2 \text{ V}^{-1} \text{ s}^{-1}$ )	$\mu_{\text{max}}$ ( $\text{cm}^2 \text{ V}^{-1} \text{ s}^{-1}$ )	$n_{\text{ref}}$ ( $\text{cm}^{-3}$ )	$\alpha$
30	580	930	$3.8 \times 10^{16}$	1.3
50	820	1750	$3.1 \times 10^{16}$	1.3
80	1040	3190	$2.3 \times 10^{16}$	1.3

increases the total scattering rate by between 2 and  $6 \times 10^{12} \text{ s}^{-1}$ . Reducing the diameter from 80 nm to 50 nm reduces the mobility by up to 45%, and reducing the diameter from 50 nm to 30 nm degrades the mobility by up to 47%.

### 3.3. Photoconductivity lifetime

It is well known that for GaAs nanowires, the photoconductivity decay rate depends approximately inversely on the nanowire diameter [7, 15]. This dependence is clear in figure 4(a) where the nanowires of the largest diameter exhibit the slowest decay. This diameter-dependence occurs because as the diameter shrinks, the likelihood of a charge carrier interacting with the nanowire surface increases, and consequently the rate of trapping and non-radiative recombination at the surface increases. The surface recombination velocity of GaAs is particularly high, making GaAs nanowire more sensitive to surface recombination than InAs and InP nanowires [7].

We measured photoconductivity dynamics for the 30 nm-, 50 nm- and 80 nm-diameter nanowires after photoexcitation with fluences between 4 and  $40 \mu\text{J cm}^{-2}$ , as exemplified in figure 4(b) for GaAs nanowires of 50 nm. In figure 4(b) the photoconductivity dynamics exhibit a rapid initial decay followed by a slower decay, and the initial decay slows with increasing fluence. This behaviour is common to all nanowires investigated regardless of diameter. In our previous publication we attributed this behaviour to surface trap states that become saturated at higher photoexcited carrier densities and at longer times after photoexcitation, slowing the decay rate [6]. Surface passivation was effective in removing these trap states [6]. In the Shockley–Read–Hall framework, the saturable traps are those that fill quickly due to their high capture cross-section for electrons, but empty slowly due to their deep nature and due to their relatively low capture cross-section for holes. To investigate the nature of trapping and the dependence of diameter, we fitted the conductivity decay data using a pair of coupled rate equations accounting for saturable and non-saturable trapping routes:

$$\frac{dn(t)}{dt} = G(t) - \frac{n(t)}{\tau_{\text{ns}}} + \frac{n(t)}{\tau_{\text{s}}(t)}, \quad (16)$$

$$\frac{dT(t)}{dt} = -\frac{d}{4} \frac{n}{\tau_{\text{s}}(t)}. \quad (17)$$

In the above,  $n(t)$  is the photoexcited electron density per unit volume,  $T(t)$  is the density of empty saturable traps per unit

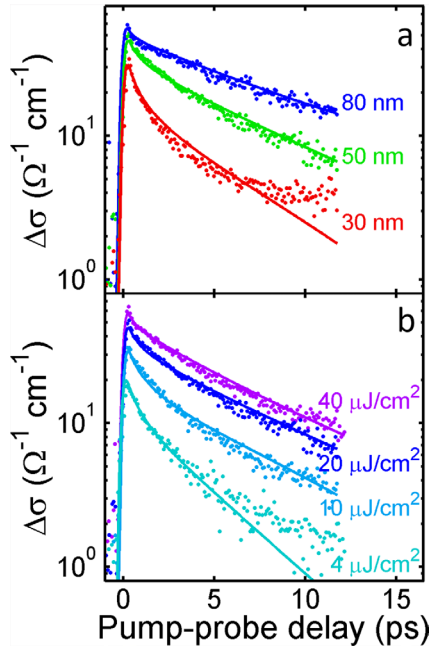


**Figure 4.** Photoinduced conductivity decays (a) in GaAs nanowires with diameters of 30 nm (red), 50 nm (green) and 80 nm (blue) after photoexcitation at a fluence of  $20 \mu\text{J cm}^{-2}$ , and (b) in nanowires of 50 nm in diameter after photoexcitation at fluences of 4, 10, 20 and  $40 \mu\text{J cm}^{-2}$ . The lines are fits obtained using the rate equations described in the text.

surface area,  $G(t)$  is the generation rate given by the photoexcitation pulse,  $\tau_{\text{ns}}$  is the electron trapping time via non-saturable recombination pathways,  $\tau_{\text{s}}(t)$  represents the electron trapping time via saturable surface traps and  $d$  is the nanowire diameter. The factor of  $d/4$  in equation (17) maintains dimensional consistency between  $n(t)$  ( $\text{cm}^{-3}$ ) and  $T(t)$  ( $\text{cm}^{-2}$ ), and was derived by modelling the nanowires as infinitely long cylinders. The value of  $\tau_{\text{s}}(t)$  depends on the fraction of saturable traps that are empty according to:

$$\tau_{\text{s}}(t) = \tau_{\text{s},0} \frac{T_0}{T(t)}, \quad (18)$$

where  $T_0$  is the total density of saturable trap states (filled or empty), and  $\tau_{\text{s},0}$  is the trapping time when all these traps are empty at time  $t = 0$ . The model is similar to the models employed by Jepsen [28] and Beaudoin [29] to describe saturable trapping in silicon nanostructures.

At the carrier densities investigated here ( $< 10^{18} \text{ cm}^{-3}$ ) the rates of Auger and bimolecular recombination are negligible compared to the rate of photoconductivity decay observed [30], and so terms for Auger and bimolecular recombination were not included in our fitting. To fit to the conductivity, the carrier density  $n$  given by the rate equations was converted to conductivity using  $\sigma = ne\mu(n)$  where  $\mu(n)$  is determined as in figure 3(a).

The surfaces of the nanowires are expected to have similar surface properties regardless of nanowire diameter. Therefore the density of surface traps  $T_0$  was used as a global fit parameter that is held constant across all diameters. The best fits were obtained with  $T_0 = (1.9 \pm 0.4) \times 10^{11} \text{ cm}^{-2}$ . The parameters  $\tau_{\text{ns}}$  and  $\tau_{\text{s},0}$  were allowed to vary with diameter and are summarised in table 2.

**Table 2.** Fit parameters describing the non-saturable and saturable electron lifetimes of nanowires with diameter 30 nm, 50 nm and 80 nm.

Diameter (nm)	$\tau_{\text{s},0}$ (ps)	$\tau_{\text{ns}}$ (ps)
30	$0.7 \pm 0.2$	$5 \pm 1$
50	$1.1 \pm 0.3$	$6 \pm 2$
80	$1.2 \pm 0.3$	$8 \pm 2$

Because the decay rate changes with carrier density and time after photoexcitation, the effective surface recombination velocity also changes. It is highest under conditions of low injected carrier densities and immediately after photoexcitation, when surface traps are unoccupied. The surface recombination velocity under moderate photoexcitation has previously been measured at  $5.4 \times 10^5 \text{ cm s}^{-1}$  [7]. To determine the upper limit of the surface recombination velocity,  $S_{\text{max}}$ , we consider the scenario when all traps are available and model the recombination time with the function [22, 31]

$$\frac{1}{\tau_{\text{volume}}} + \frac{4S_{\text{max}}}{d} = \frac{1}{\tau_{\text{ns}}} + \frac{1}{\tau_{\text{s},0}}, \quad (19)$$

where  $\tau_{\text{volume}}$  is the time constant for recombination in the nanowire volume that cannot be attributed to surface recombination phenomena. We use a value of 1.6 ns to model  $\tau_{\text{volume}}$ , which is the lifetime observed in well-passivated GaAs nanowires [12]. We fitted equation (19) to the parameters in table 2 to calculate a maximum surface recombination velocity of  $1.3 \times 10^6 \text{ cm s}^{-1}$ . The lower limit, when all saturable traps are filled, is calculated as  $S_{\text{min}} = 1.7 \times 10^5 \text{ cm s}^{-1}$ .

Finally, we note that the properties of bare intrinsic GaAs nanowires under investigation here differ significantly from those of doped GaAs nanowires investigated previously [32]. Doped nanowires exhibit much longer photoconductivity lifetimes, as doping modifies the band-bending at the nanowire surface to reduce the rate of surface recombination [32].

## 4. Conclusion

The conductivity of intrinsic GaAs nanowires is strongly influenced by surface scattering mechanisms and surface states. Using OPTP spectroscopy, we have measured photoconductivity dynamics and charge carrier transport on picosecond timescales. Due to surface scattering, the electron mobility is strongly degraded as the nanowire diameter is reduced. Compared to 80 nm diameter nanowires, nanowires with diameters of 50 nm and 30 nm suffer additional surface-related scattering at rates of  $7 \times 10^{12} \text{ s}^{-1}$  and  $20 \times 10^{12} \text{ s}^{-1}$  respectively. The nanowires exhibit high surface recombination velocities between  $1.7 \times 10^5 \text{ cm s}^{-1}$  and  $1.3 \times 10^6 \text{ cm s}^{-1}$ , with the upper limit occurring when saturable surface traps are unoccupied and the lower limit occurring when these traps are filled.

These findings are of importance for engineering high speed nanowire-based optoelectronic devices, for which short carrier lifetimes and high mobilities are highly desirable characteristics. With increasing GaAs nanowire diameter, the mobility increases but the lifetime also increases, so when

selecting the nanowire geometry there must be a compromise between achieving a short lifetime and a high carrier mobility. We note that an alternative parameter controlling the mobility and lifetime is the charge carrier density. As the carrier density is reduced, the mobility increases and the lifetime is reduced. Therefore, to achieve high speed GaAs nanowire devices, we propose operating the devices under low injection conditions at which charge carrier mobility is maximal.

### Acknowledgments

The authors gratefully acknowledge EPSRC (UK) (HJJ, JLB, SAB LMH, MBJ) and the Australian Research Council (HHT and CJ) for research funding. H J Joyce gratefully acknowledges the Royal Commission for the Exhibition of 1851 for her research fellowship. The Australian National Fabrication Facility, ACT Node, is acknowledged for access to the growth facility used in this work. Data sets related to this publication are available from the University of Cambridge data repository at <https://doi.org/10.17863/CAM.9203>.

### Appendix

To derive equations (3) and (4) we consider the electric fields transmitted through the nanowires ( $E_w$ ), through the photoexcited nanowires ( $E_w^*$ ), and through the vacuum surrounding the nanowires ( $E_v$ ):

$$\frac{E_w(\omega)}{E_v(\omega)} = \frac{t_{vw}t_{ws}}{t_{vs}} \exp\left(\frac{i\omega d}{c}(\tilde{n}_w - \tilde{n}_v)\right) \frac{FP_{vws}FP_{wsv}}{FP_{vsv}} \quad (\text{A.1})$$

$$\frac{E_w^*(\omega)}{E_w(\omega)} = \frac{t_{vw}^*t_{ws}^*}{t_{vw}t_{ws}} \exp\left(\frac{i\omega d}{c}(\tilde{n}_w^* - \tilde{n}_w)\right) \frac{FP_{vws}^*FP_{wsv}^*}{FP_{vws}FP_{wsv}} \quad (\text{A.2})$$

In the above  $t_{ij} = 2\tilde{n}_i/(\tilde{n}_i + \tilde{n}_j)$  are the Fresnel transmission coefficients when passing from layer  $i$  to layer  $j$ ,  $\tilde{n}_i$  are the complex refractive indices,  $c$  is the speed of light in vacuum,  $d$  is the thickness of the layer containing the nanowires,  $*$  denotes the photoexcited case, and the subscripts  $v$ ,  $w$  and  $s$  denote the vacuum, nanowire and substrate respectively. The Fabry–Pérot terms  $FP_{ijk}$  account for the internal reflections within layer  $j$ :

$$FP_{ijk} = \sum_{p=0}^P \left[ r_{jk}r_{ji} \exp\left(\frac{2i\tilde{n}_j\omega d_j}{c}\right) \right]^p, \quad (\text{A.3})$$

where  $r_{ij} = (\tilde{n}_i - \tilde{n}_j)/(\tilde{n}_i + \tilde{n}_j)$  are the Fresnel reflection coefficients and  $d_j$  is the thickness of the layer. The summation limit  $P$  is set by the number of internal reflections recorded in the waveforms.

The derivation of equation (3) from equation (A.1) can be found in [23]. In a similar fashion, equation (A.2) can be simplified to equation (4) using the following approximations. Firstly, the substrate is very thick compared to the wavelength of the THz radiation ( $d_s > \lambda_{\text{THz}}$ ) so we may invoke the thick film approximation ( $P = 0$ ) to obtain  $FP_{vsv}$ ,  $FP_{wsv}$ ,  $FP_{wsv}^* = 1$ . Secondly, the nanowires are very thin ( $d_1 \ll \lambda_{\text{THz}}$ ) so we may use the thin film

limit ( $P \rightarrow \infty$ ) to obtain  $FP_{vws} = (1 - r_{ws}r_{wv} \exp(2i\tilde{n}_w\omega d/c))^{-1}$  and  $FP_{vws}^* = (1 - r_{ws}^*r_{wv}^* \exp(2i\tilde{n}_w^*\omega d/c))^{-1}$ . In addition, as the nanowires are thin, we make the approximation  $\exp(\pm i\tilde{n}_w\omega d/c) \approx 1 \pm i\tilde{n}_w\omega d/c$ . Applying these simplifications to equation (A.2) yields:

$$\frac{E_w^*(\omega)}{E_w(\omega)} = \frac{\tilde{n}_v + \tilde{n}_s - \frac{i\omega d}{c}(\tilde{n}_w^2 + \tilde{n}_v\tilde{n}_s)}{\tilde{n}_v + \tilde{n}_s - \frac{i\omega d}{c}(\tilde{n}_w^{*2} + \tilde{n}_v\tilde{n}_s)} \quad (\text{A.4})$$

and substituting  $\tilde{n}_v = 1$ ,  $\epsilon_w = \tilde{n}_w^2$  and  $\epsilon_w^* = \tilde{n}_w^{*2}$  yields equation (4).

### References

- [1] Aberg I *et al* 2016 A GaAs nanowire array solar cell with 15.3% efficiency at 1 sun *IEEE J. Photovolt.* **6** 185–90
- [2] Yao M, Cong S, Arab S, Huang N, Povinelli M L, Cronin S B, Dapkus P D and Zhou C 2015 Tandem solar cells using GaAs nanowires on Si: design, fabrication, and observation of voltage addition *Nano Lett.* **15** 7217–24
- [3] Heiss M *et al* 2013 Self-assembled quantum dots in a nanowire system for quantum photonics *Nat. Mater.* **12** 439–44
- [4] Saxena D, Mokkapati S, Parkinson P, Jiang N, Gao Q, Tan H H and Jagadish C 2013 Optically pumped room-temperature GaAs nanowire lasers *Nat. Photon.* **7** 963–8
- [5] Peng K *et al* 2015 Single nanowire photoconductive terahertz detectors *Nano Lett.* **15** 206–10
- [6] Parkinson P, Joyce H J, Gao Q, Tan H H, Zhang X, Zou J, Jagadish C, Herz L M and Johnston M B 2009 Carrier lifetime and mobility enhancement in nearly defect-free core-shell nanowires measured using time-resolved terahertz spectroscopy *Nano Lett.* **9** 3349–53
- [7] Joyce H J, Docherty C J, Gao Q, Tan H H, Jagadish C, Lloyd-Hughes J, Herz L M and Johnston M B 2013 Electronic properties of GaAs, InAs and InP nanowires studied by terahertz spectroscopy *Nanotechnology* **24** 214006
- [8] Titova L V, Hoang T B, Jackson H E, Smith L M, Yarrison-Rice J M, Kim Y, Joyce H J, Tan H H and Jagadish C 2006 Temperature dependence of photoluminescence from single core-shell GaAs-AlGaAs nanowires *Appl. Phys. Lett.* **89** 173126
- [9] Ketterer B, Uccelli E and Fontcuberta i Morral A 2012 Mobility and carrier density in p-type GaAs nanowires measured by transmission Raman spectroscopy *Nanoscale* **4** 1789–93
- [10] Parkinson P, Lloyd-Hughes J, Gao Q, Tan H H, Jagadish C, Johnston M B and Herz L M 2007 Transient terahertz conductivity of GaAs nanowires *Nano Lett.* **7** 2162–5
- [11] Perera S *et al* 2008 Nearly intrinsic exciton lifetimes in single twin-free GaAsAlGaAs core-shell nanowire heterostructures *Appl. Phys. Lett.* **93** 053110
- [12] Joyce H J, Parkinson P, Jiang N, Docherty C J, Gao Q, Tan H H, Jagadish C, Herz L M and Johnston M B 2014 Electron mobilities approaching bulk limits in ‘surface-free’ GaAs nanowires *Nano Lett.* **14** 5989–94
- [13] Boland J L *et al* 2015 Modulation doping of GaAs/AlGaAs core-shell nanowires with effective defect passivation and high electron mobility *Nano Lett.* **15** 1336–42
- [14] Yong C K, Noori K, Gao Q, Joyce H J, Tan H H, Jagadish C, Giustino F, Johnston M B and Herz L M 2012 Strong carrier lifetime enhancement in GaAs nanowires coated with semiconducting polymer *Nano Lett.* **12** 6293–301
- [15] Demichel O, Heiss M, Bleuse J, Mariette H and Fontcuberta i Morral A 2010 Impact of surfaces on the optical properties of GaAs nanowires *Appl. Phys. Lett.* **97** 201907

- [16] Chang C C *et al* 2012 Electrical and optical characterization of surface passivation in GaAs nanowires *Nano Lett.* **12** 4484–9
- [17] Zhang J, Chia A C E and LaPierre R R 2014 Low resistance indium tin oxide contact to n-GaAs nanowires *Semicond. Sci. Technol.* **29** 54002
- [18] Suyatin D B *et al* 2014 Strong Schottky barrier reduction at Au-catalyst/GaAs-nanowire interfaces by electric dipole formation and Fermi-level unpinning *Nat. Commun.* **5** 3221
- [19] Gutsche C, Lysov A, Regolin I, Brodt A, Liborius L, Frohleiks J, Prost W and Tegude F J 2011 Ohmic contacts to n-GaAs nanowires *J. Appl. Phys.* **110** 014305
- [20] Joyce H J, Gao Q, Tan H H, Jagadish C, Kim Y, Zhang X, Guo Y and Zou J 2007 Twin-free uniform epitaxial GaAs nanowires grown by a two-temperature process *Nano Lett.* **7**
- [21] Jiang N, Wong-Leung J, Joyce H J, Gao Q, Tan H H and Jagadish C 2014 Understanding the true shape of Au-catalyzed GaAs nanowires *Nano Lett.* **14** 5865–72
- [22] Joyce H J *et al* 2012 Ultralow surface recombination velocity in InP nanowires probed by terahertz spectroscopy *Nano Lett.* **12** 5325–30
- [23] Joyce H J, Boland J L, Davies C L, Baig S and Johnston M B 2016 A review of the electrical properties of semiconductor nanowires: insights gained from terahertz conductivity spectroscopy *Semicond. Sci. Technol.* **31** 103003
- [24] Strait J H, George P A, Levendorf M, Blood-Forsythe M, Rana R and Park J 2009 Measurements of the carrier dynamics and terahertz response of oriented germanium nanowires *Nano Lett.* **9** 2967–72
- [25] Joyce H J *et al* 2008 High purity GaAs nanowires free of planar defects: growth and characterization *Adv. Funct. Mater.* **18** 3794–800
- [26] Venermo J and Sihvola A 2005 Dielectric polarizability of circular cylinder *J. Electrostat.* **63** 101–17
- [27] Chou L W, Shin N, Sivaram S V and Filler M A 2012 Tunable mid-infrared localized surface plasmon resonances in silicon nanowires *J. Am. Chem. Soc.* **134** 16155–8
- [28] Uhd Jepsen P, Schairer W, Libon I H, Lemmer U, Hecker N E, Birkholz M, Lips K and Schall M 2001 Ultrafast carrier trapping in microcrystalline silicon observed in optical pump-terahertz probe measurements *Appl. Phys. Lett.* **79** 1291–3
- [29] Beaudoin A, Salem B, Baron T, Gentile P and Morris D 2014 Impact of n-type doping on the carrier dynamics of silicon nanowires studied using optical-pump terahertz-probe spectroscopy *Phys. Rev. B* **89** 115316
- [30] Strauss U, Rühle W W and Köhler K 1993 Auger recombination in intrinsic GaAs *Appl. Phys. Lett.* **62** 55–7
- [31] Léonard F, Talin A A, Swartzentruber B S and Picraux S T 2009 Diameter-dependent electronic transport properties of Au-catalyst/Ge-nanowire Schottky diodes *Phys. Rev. Lett.* **102** 106805
- [32] Boland J L *et al* 2016 Increased photoconductivity lifetime in GaAs nanowires by controlled n-type and p-type doping *ACS Nano* **10** 4219–27